PHOTO-INDUCED AND ELECTROOPTIC PROPERTIES OF (Pb,La)(Zr,Ti)O_3 FILMS FOR OPTICAL MEMORIES

D. DIMOS, B.G. POTTER, M.B. SINCLAIR, B.A. TUTTLE, and W.L. WARREN
Sandia National Laboratories, Albuquerque, NM 87185

Abstract Photo-induced hysteresis changes and electrooptic effects in sol-gel Pb(Zr,Ti)O_3 (PZT) and PLZT films have been studied in an effort to evaluate these materials for optical memory applications. The films exhibit two types of photo-induced changes in their hysteresis behavior which are suitable for optical storage. Both types of photo-induced hysteresis changes are due to trapping of photo-generated charge carriers at sites which minimize internal depolarizing fields. The photo-induced changes are reproducible and stable, which indicates that the charge traps are stable. However, improvements in photosensitivity will be required to develop a competitive technology for optical memories. In addition, polarization-dependent changes in the refractive indices can be the basis of a nondestructive optical readout technique. The index changes of films have been determined using a waveguide refractometry technique, which allows the extraordinary and ordinary index changes to be obtained independently.

INTRODUCTION

There is an increasing demand today for devices capable of storing and processing large quantities of optical information, including random-access optical memories, image comparators, and spatial light modulators (SLMs). Ferroelectric thin films, especially those based on PLZT solid solutions, exhibit photo-induced and electrooptic responses that make them promising materials for optical-information storage, display and processing applications [1-5].

To store optically-generated information, near-band-gap light is used, in possible combination with an applied bias, to locally modify the polarization state of the film. This type of photoferroelectric effect has been extensively studied in PLZT ceramics [6-8]; however, relatively little has been reported about comparable effects in ferroelectric films [9,10]. In this paper, the types of photo-induced changes that are observed in the hysteresis behavior of PZT and PLZT films are reported. Both the mechanisms responsible for these effects and their potential utility in optical memory devices are discussed.

For optical readout, the polarization-dependent birefringence can be used to modulate the reflected (or transmitted) light intensity. A number of studies of electrooptic responses of PZT and PLZT films have shown that thin-film electrooptic properties are comparable to PLZT ceramics [11-14]. However, previous measurements of the electrooptic response of P(L)ZT films have only measured changes in birefringence ($\Delta n_e - \Delta n_o$). Refractometry, based on prism coupling into thin-film waveguide modes, is an alternative technique for evaluating optical

and electroptic properties that permits a determination of the individual contributions to the induced birefringence. These measurements can thus provide more detailed information about the mechanisms that contribute to the electrooptic response.

EXPERIMENTAL

PZT and PLZT films were fabricated by spin coating using a metal alkoxide solution; the precursors were lead (IV) acetate, lanthanum acetate, zirconium butoxide-butanol, and titanium isopropoxide. A comprehensive description of the procedure has been previously published [15,16]. The desired film thickness was achieved by depositing multiple layers. After each layer, a 300°C bake was used to drive off volatile organics. Oxidized silicon wafers and MgO single crystals were used as substrates. The base electrode was either Pt or RuO_x ($x \leq 2$), which gave four different substrate types: $Pt/Ti/SiO_2/Si$, $RuO_x/Ti/SiO_2/Si$, Pt/MgO, and $RuO_x/Ti/MgO$; the Ti layer was to promote adhesion. For the Pt/MgO samples, the Pt was deposited at roughly 600°C to achieve a high degree of [100] orientation. The films on Si subtrates were fired at 650°C for about 30 min. The films on MgO substrates were processed using rapid thermal annealing to 650°C; a highly-oriented [001] PZT film was obtained with the oriented Pt electrode. Both procedures yielded films that were essentially single-phase perovskite and had columnar microstructures with a lateral grain size of 100-150 nm. Films in excess of 500 nm thick were prepared by firing after every 4 layers to avoid cracking during densification.

Top electrodes (1-3 mm diameter) were sputter deposited to establish parallel-plate capacitors. To investigate photo-induced effects, optically-transparent indium tin oxide (ITO) or thin, semi-transparent metal films were used. A 10 nm thick Pt film was typically used for the top electrode, since Pt gave the most reproducible electrical properties; however, thin Au (10 nm), RuO_x (20 nm), and ITO (150 nm) electrodes were also used for comparison.

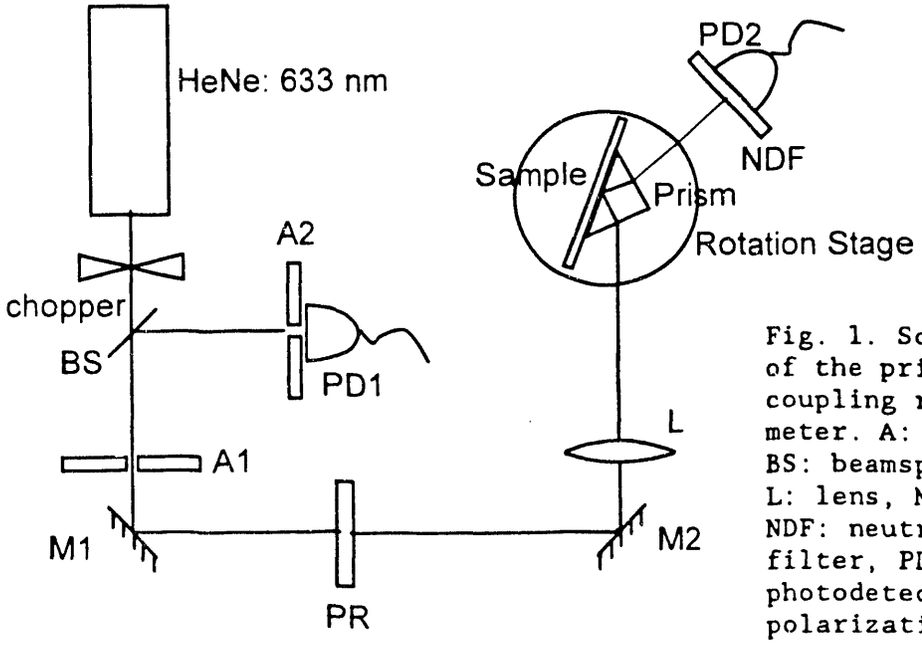

Fig. 1. Schematic of the prism-coupling refracto-meter. A: aperture BS: beamsplitter, L: lens, M: mirror, NDF: neutral density filter, PD: silicon photodetector, PR: polarization rotator

Hysteresis loops for the films were measured using the RT-66A tester (Radiant Tech.). A 200 W Oriel Hg arc lamp in combination with narrow band interference filters and a frequency-doubled Ti-sapphire laser were used to generate UV and near-UV illumination for studying photo-induced effects. The illumination intensity was adjusted using neutral density filters. An Ealing optical shutter, which also triggered a voltage supply, was used to control the exposure time.

Electrooptic measurements were made using a prism-coupling refractometer, as shown in Fig. 1. The sample was clamped to the hypotenuse of a right-angle rutile prism. A HeNe laser (633 nm) was focused through the prism onto the sample/prism coupling spot. The sample/prism arrangement was mounted onto a computer-interfaced rotation stage which controlled the incidence angle. The reflected beam intensity was measured with a Si photodiode and a chopper/lock-in amplifier combination to achieve phase-sensitive detection. TE and TM incident polarization states were selected using a polarization rotator. Additional details have been presented elsewhere [17].

PHOTO-INDUCED EFFECTS

All PZT and PLZT films exhibit two primary effects that can be used to store optically-generated information. The first effect is a photo-induced shift of the hysteresis loop along the voltage axis, which is illustrated in Fig. 2 for a $Pb(Zr_{0.4}Ti_{0.6})O_3$ (PZT 40/60) film (420 nm thick) on Pt/MgO. A fairly square hysteresis loop is obtained since the film is both highly oriented and compressively stressed, due to the thermal expansion mismatch with the substrate [18,19]. The two curves for $+V_s$ and $-V_s$ were obtained by biasing the top electrode at +6V and -6V, respectively, while illuminating the capacitor with band-gap light (365 nm). The translation of the hysteresis loop implies that a photo-induced, space-charge field has been introduced into the film. The two states obtained with the saturating voltages are stable

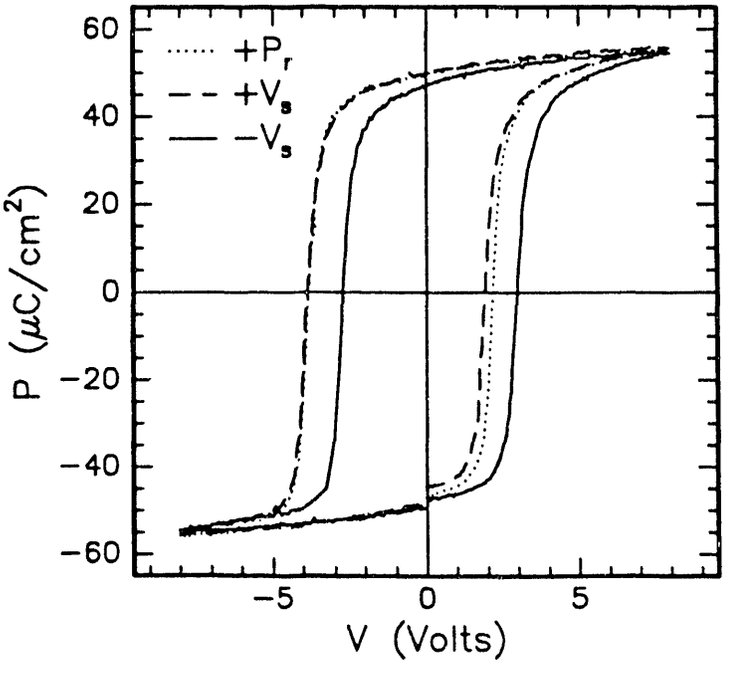

Figure 2. Photo-induced voltage shift for $+P_r$, $+V_s$, $-V_s$. PZT 40/60 film on Pt/MgO (420 nm). $|V_s|$ = 6V, λ = 365 nm, I = 25 mW/cm^2, t = 20 sec.

and reproducible end-point states and thus can be the basis of an optical memory device, as discussed later. In addition, Fig. 2 shows the loop obtained after a sample which displayed the $-V_s$ behavior was switched to $+P_r$ and then illuminated at zero bias. The hysteresis loop obtained this way is essentially the same as that obtained with a positive saturating bias and light. This result shows that the voltage shift is derived from the polarization state of the material rather than the applied bias. This conclusion is consistent with the observation that the value of ΔV_c does not increase with increasing bias as long as the bias is sufficient to cause complete switching.

The other phenomenon exhibited by all films is a photo-induced suppression of the dynamic polarization range, as illustrated in Fig. 3. The dashed line gives the initial hysteresis response for this sample, which is a PZT 53/47 film (810 nm thick) on $Pt/Ti/SiO_2/Si$. After poling the test capacitor to the negative remanent polarization value, $-P_r$, it was illuminated with band-gap light for 10 sec with a bias of +2.5 V, which is near the switching threshold. Under these conditions, the hysteresis response (solid line) exhibited not only a noticeable change in the coercive voltage, V_c, but also a clear suppression in the switchable polarization at saturation, ΔP_s, and at remanence, ΔP_r. The solid curve, which is the new steady-state response, was obtained following several post-illumination hysteresis cycles. This procedure was used because some recovery of the dynamic polarization range, ΔP_s (ΔP_r), occurs during the first few cycles. Suppression of the switchable polarization was only observed for biases that lead to partial switching, in contrast to the behavior observed for biases that cause complete switching (Fig. 2), where a pure voltage shift is obtained without suppression of ΔP_s or ΔP_r.

The photo-induced change in remanent polarization, δP_r, from the unilluminated to the illuminated response, which is most apparent for this sample at $-P_r$, could also be the basis of an optical memory. The amount by which the polarization ranges, ΔP_s and ΔP_r, are suppressed is a sensitive function of bias voltage and is maximized by partially switching with a bias just below V_c. Larger photo-induced changes in ΔP_s and ΔP_r, than seen in Fig. 3, have been obtained for samples with

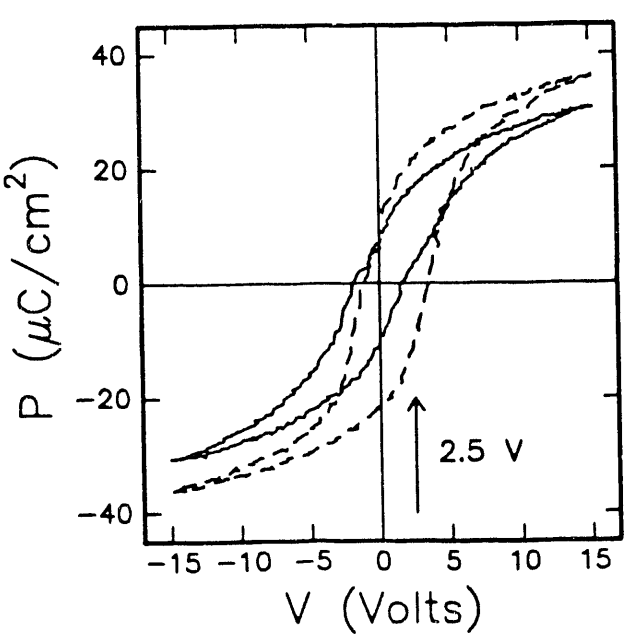

Figure 3. Photo-induced suppression of ΔP_s (ΔP_r) by partial switching. PZT 53/47 (810 nm) on $Pt/Ti/SiO_2/Si$. .... initial response. ____ after optical writing. V = +2.5 V, t = 10 sec, λ = 365 nm, I = 25 mW/cm^2.

higher initial values of ΔP_s and ΔP_r. The reduction in the values of ΔP_s or ΔP_r can be regarded as a photo-induced analog of fatigue. The initial hysteresis response can be restored by illuminating the sample with a saturating bias of the opposite sign ($-V_s$). Some recovery of ΔP_s (ΔP_r) also occurs at $+V_s$, but the restoration is typically incomplete. Photo-induced fatigue effects have also been observed when storing optical images in bulk-ceramic samples of PLZT [8,20].

Another effect related to the restoration of an optically fatigued sample has been commonly observed in previously untested samples. It was found that the initial values of ΔP_s and ΔP_r are improved by applying a saturating bias with band-gap light [21]. The observation of a photo-induced improvement in the initial hysteresis response suggests that processing can produce an effect similar to optical fatigue. The improvement obtained is comparable to the increase in ΔP_r typically seen during the early stage of electrical fatigue.

The photo-induced changes in hysteresis can be qualitatively accounted for by considering the interaction between internal fields due to the polarization charge and photo-generated carriers. The situation that occurs due to a saturating bias will be considered initially. A reasonable domain configuration for an unoriented, columnar film that has been poled is schematically depicted in Fig. 4. The arrow head represents the positive end of the spontaneous dipole. The internal charge separation would lead to a strong depolarizing field, except for the fact that an opposing charge builds up on the electrodes to compensate the polarization charge, which reduces the depolarizing field. However, the depolarizing field is not eliminated by the compensating charge, since some spatial separation exists between the dipole charge and the compensating charge. Illuminating the ferroelectric with band-gap light generates electron-hole pairs. The residual depolarizing field acts as a bias to redistribute the photo-generated carriers (+,-), as illustrated. Significant charge redistribution upon illumination is evidenced by the appearance of a transient photocurrent. Trapping of this charge stabilizes the present domain configuration over the oppositely oriented one, which is equivalent to introducing a space-charge field, as shown. This space-charge field leads to the observed shift of the hysteresis loop.

Since the principal polarization discontinuity occurs at the top and bottom electrode interfaces, the photo-generated carriers should become trapped near these interfaces. By assuming that the trapped charge is at or near the interfaces, ΔV_c is approximately given by,

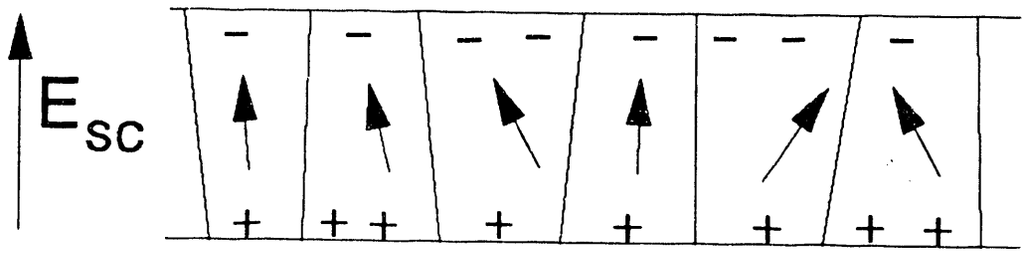

Figure 4. Schematic diagram showing the dipole orientation due to a saturating bias and the internal compensating charge.

$$\Delta V_c = (Q_+(\text{bottom}) + Q_-(\text{top})) * t/\varepsilon\varepsilon_o \ , \qquad (1)$$

where Q is the charge/unit area and t is the film thickness. According to Eq. 1, the value of ΔVc should increase linearly with thickness for similar films. Using films with various thicknesses, compositions, electrode materials, and substrate types, it was found that the value of ΔV_c increased roughly linearly with thickness, as expected, and that for films of a given thickness range, ΔV_c did not depend strongly on composition, electrode material, or substrate type [20]. The effective charge/unit area was then calculated using Eq. 1. For a 780 nm thick PZT 40/60 sample on MgO, $\Delta V_c = 1.42$ V and $\varepsilon \simeq 1000$. Assuming $Q_+ \simeq Q_-$, the effective density of trapped charge near each interface is roughly $5\times10^{12}/cm^2$, which is less than 0.1% of the available sites. This charge density is equivalent to $< 1\mu C/cm^2$, which means that the internally trapped charge compensates only a small fraction of the remanent polarization. It should also be noted that although Eq. 1 assumes trapping of both electrons and holes, the phenomenon can be sufficiently explained by trapping of primarily one charged species.

The photo-induced fatigue of Fig. 3 can be accounted for by considering the situation that occurs due to partial switching at intermediate biases. Figure 5 depicts a possible domain configuration for a sample with a macroscopic remanent polarization of roughly zero. Photo-generated charge accumulates at domain boundaries with a large polarization discontinuity. This trapped charge inhibits these domains from reorienting. By "locking" the orientation of certain domains, the switchable polarization is reduced. In addition, illumination may allow domain configurations to be established which would usually be unachieveable. For example, the head-to-head orientation, which may be possible in thick films, would normally be energetically unfavorable. However, this configuration can be stabilized by trapped electrons, as shown. Restoration of the suppressed loop requires near-band-gap light to generate new carriers, which recombine with the trapped charge, allowing the previously locked domains to be reoriented. The ability to improve the initial hysteresis response suggests that trapped charge, which can lock some domains, is introduced during processing and is eliminated, or redistributed, by illuminating under bias.

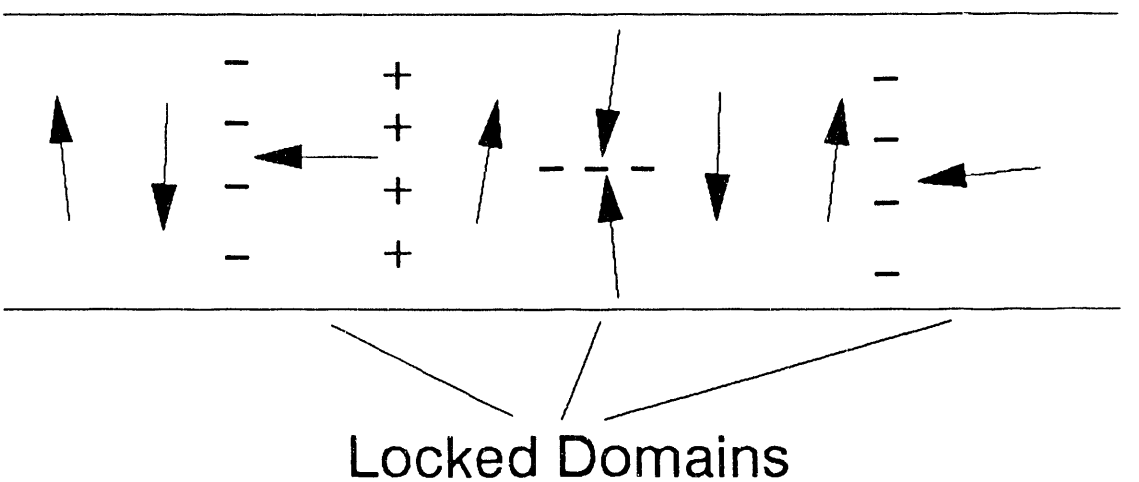

Figure 5. Schematic diagram showing a possible domain configuration for P $\simeq$ 0 and the trapped, compensating charge at domain boundaries.

Two critical parameters that characterize the photosensitivity are the dependence of the photo-induced hysteresis changes on exposure time and light energy. The spectral dependence is characterized by a peak in the photosensitivity at roughly the band edge (~ 3.4 eV) [21], and a steady drop with decreasing light energy. The kinetic response of the voltage-shift effect (Fig. 2) was determined by measuring the change in coercive voltage obtained when switching from one end-point state to the other as a function of exposure time. Figure 6 illustrates a typical result, which was obtained for a 780 nm thick PZT 40/60 film on oriented Pt/MgO. In general, the voltage-shift kinetics follow a stretched-exponential function of the form,

$$\Delta V_c(t) = \Delta V_c^{sat} [1-\exp-(t/\tau)^{\beta}] \quad . \quad (2)$$

Both the stretching parameter, β, and the relaxation time, τ, vary somewhat for different samples; τ is also a function of light intensity, wavelength, and temperature. For the conditions used in Fig. 6 (T = 21°C, λ = 365 nm, and J = 25 mW/cm^2), β = 0.53 and τ = 0.9 sec. Increasing the temperature to 80°C decreased the relaxation time to τ = 0.3 sec. Increasing the illumination intensity to 800 mW/cm^2 (390 nm, 21°C) decreased the relaxation time to 0.1 sec. The complete time dependence for the optical-fatigue effect was not characterized; however, a relaxation time comparable to that obtained for the voltage shift was consistent with qualitative observations.

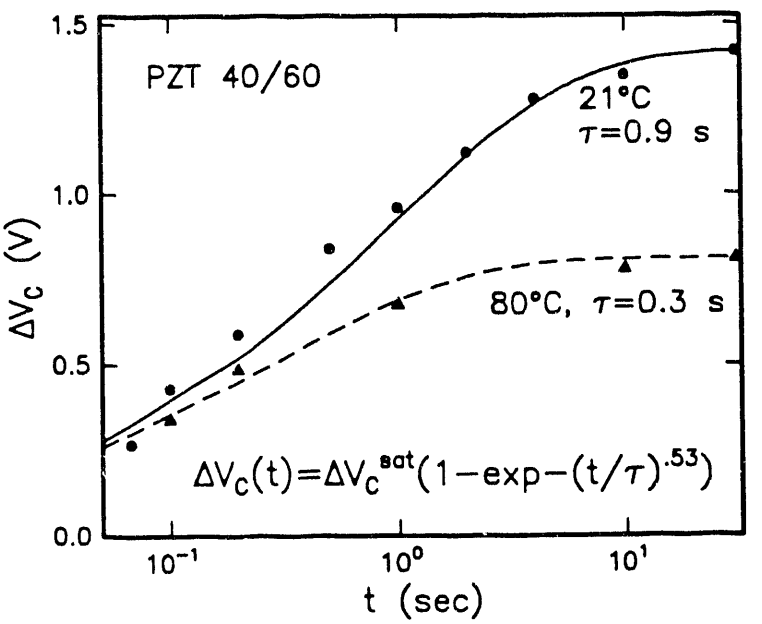

Figure 6. Voltage shift as a function of exposure time for a PZT (40/60) film (780 nm) on Pt/MgO. λ = 365 nm, I = 25 mW/cm^2. The lines are fits to the stretched exponential function (Eq. 2).

The time response may either be controlled by the carrier mobility or the charge-trapping kinetics. If charge migration is rate limiting, the stretched exponential behavior indicates a dispersive transport mechanism. In fact, a low hole mobility is anticipated due to an abundance of shallow hole traps [22,23]. Alternatively, the trapping kinetics of one or both carrier types into the deeper, more stable traps may be rate limiting. In either case, the stretched-exponential kinetics implies a distribution of trapping energies.

ELECTROOPTIC EFFECTS

Both the tetragonal and rhombohedral phases of PLZT are structurally and, thus, optically uniaxial and negatively birefringent. In addition to the uniaxial nature of individual domains, polycrystalline PLZT samples are macroscopically uniaxial, where the optic axis is parallel to applied field. Previous studies have shown that the birefringence of PZT films, $\Delta n = \Delta(n_e - n_o)$, is roughly a quadratic function of the polarization [24]. Consequently, changes in birefringence can be used to monitor changes in the polarization state of the film. To obtain more detailed information about the electrooptic response, we have recently measured the field-induced changes in the extraordinary and ordinary indices, Δn_o and Δn_e, using the prism-coupling refractometer [17]. This technique was used to determine not only the birefringence, but also the changes in the principal indices that contribute to Δn.

Typical scans of the reflectivity as a function of incidence angle are given in Figs. 7a and b for TE and TM polarized light, respectively. The sample is a PZT 53/47 film (810 nm thick) on a $Pt/Ti/SiO_2/Si$ substrate with a semi-transparent Ag electrode. Drops in the reflected intensity are associated with waveguiding modes. For TE polarization, the index in the plane of the film, n_o, determines the waveguiding conditions. For TM polarization, waveguiding conditions are determined by both n_o and the out-of-plane index (n_e). Using known

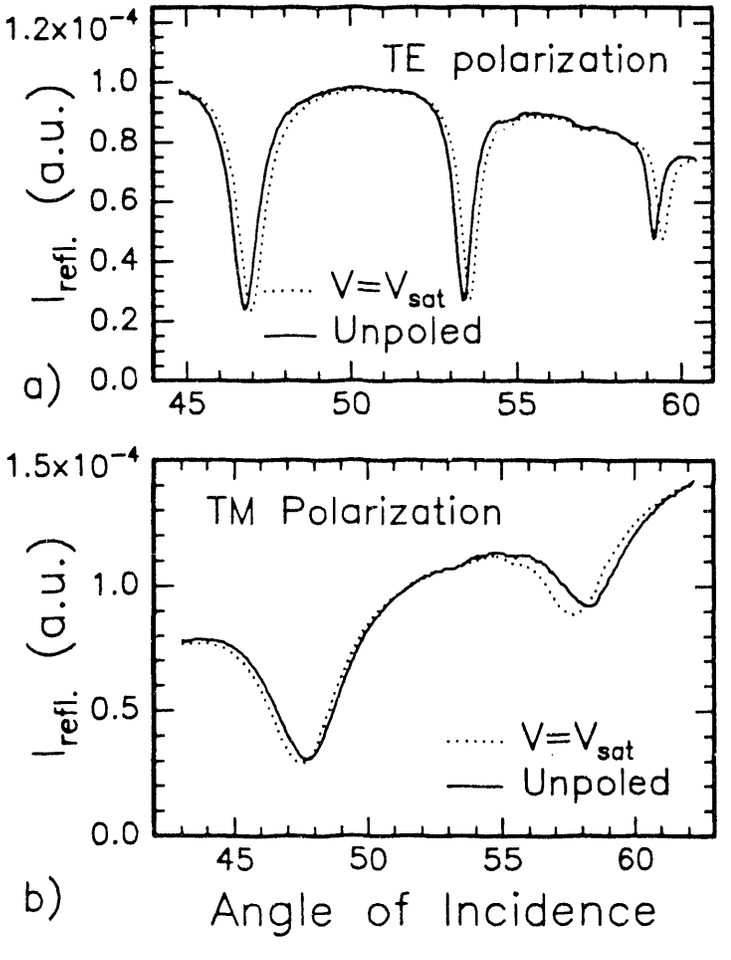

Figure 7. Scans of the reflectivity as a function of incidence angle for $P_r \simeq 0$ and $P = P_{sat}$; a) TE polarization; b) TM polarization.

or measured optical constants for the electrodes and prism, the indices and thickness of the PZT film can be determined by fitting the reflectivity curves. This technique is most accurate for films that generate at least three modes so that the fit is overconstrained.

The solid curves in Figs. 7a and b were obtained at zero bias after switching the sample to a zero remanent polarization state ($P_r \simeq 0$). The values of the film thickness and in-plane index obtained using the TE polarization scan were t = 828 nm and n_o = 2.544. Using this value for n_o, the thickness and out-of-plane index obtained from fitting the TM scan were t = 825 nm and n_e = 2.547. Within the degree of uncertainty inherent in these fits, this data indicates that the film is nearly optically isotropic at P_r = 0. The film thickness values were also in good agreement with each other and with the value obtained using a Dektak profilometer (t ≃ 810 nm).

The dashed curves in these figures correspond to scans with an applied dc voltage of 10 V (E ≃ 125 kV/cm); this voltage was sufficient to saturate the polarization. From the TE scan, the ordinary index was found to have increased by 0.004 (n_o = 2.548). Using this value for Δn_o, the change in the extraordinary index determined using the TM curve at 10 V was -0.017 (n_e = 2.530). As expected, the applied field leads to a negative birefringence [14]. The measured change in birefringence of $\Delta(n_e-n_o)$ = -0.210 is also similar to values recently reported for other PZT films [11,12]. Although the absolute index and thickness values for the PZT are sensitive to uncertainties in the electrode indices, the field-induced index changes are relatively insensitive to the fitting parameters, which lends additional confidence to the values obtained for Δn_o and Δn_e. An increase in the film thickness of about 2 nm was also indicated by fitting the applied field response. A beam deflection technique, which directly measured changes in the film thickness, was used to verify a thickness change of this magnitude [17].

In addition, the waveguide measurement indicates that the ratio of $\Delta n_e/\Delta n_o$ is roughly -4/1. A theoretical expression for this ratio can be obtained by considering the reorientation of the individual domains by the electric field. In the unpoled state, the domains are assumed to be randomly oriented leading to optically isotropic behavior. The electric field tends to align the domains which results in negative birefringence at remanence, with $\Delta n_e/\Delta n_o$ = -2/1 [17,14]. One difference between this calculation and the present experiment is that the index measurements were made with an applied field, which is likely to modify the calculated ratio for the remanent condition due to the linear electrooptic effect. The ratio can also be affected by a strain-optic effect which can occur due to clamping of the film by the substrate. Thus, this measurement provides information about the importance of mechanisms other than simple domain reorientation.

CONSIDERATIONS FOR OPTICAL STORAGE DEVICES

Optical memories have several inherent advantages over electronic or magnetic memories. First, the minimum bit size for an optical memory is comparable to the wavelength of light, which translates into very high storage densities ($\geq 10^7/cm^2$). Second, optical systems have high numerical apertures, which make them more tolerant to dust, scratches, and vibration than magnetic memories. Third, optical disks for

computers are removable, unlike magnetic hard disks, which make optical disks ideal for archival storage. The primary requirements for an optical memory medium are that light can be used to produce a change in the state of the material and that the states can be differentiated optically. As previously shown, light can be used to produce stable and reproducible changes in the polarization state of P(L)ZT films and light can be used to determine the local polarization state based on the polarization-dependent birefringence. Consequently, P(L)ZT films satisfy the requirements for an optical storage medium. In comparison to magnetooptic (MO) memories, P(L)ZT thin-film memories will have a wider operating temperature range because of their higher Curie temperatures ($T_c \simeq 350°$-$400°C$ for PZT vs $T_c \simeq 100°$-$150°C$ for MO materials). In addition, optical storage in P(L)ZT is an electronic effect as opposed to the thermal effect used in MO memories. Hence, ferroelectric memories could use more reliable, low power lasers.

A simple operational scheme for a digital optical memory is illustrated in Fig. 8. Initially the entire PZT film is reset to the positive curve (+) by switching to $+P_r$ and illuminating. The film is then electrically switched to $-P_r$ with no light. Individual bits are switched to the negative curve (-) by illuminating them one at a time; this procedure allows the bits to be completely defined by the optical addressing process. However, both the illuminated and unilluminated bits are still at $-P_r$. To read the stored information, a bias is applied to the entire film that partially switches the (+) bits while leaving the (-) bits at $-P_r$. In this case, a pulse (10 sec) at 3.7 V switches the (+) bits to $P_r \simeq 0$, as illustrated with the dotted curve. This step illustrates the advantage of having a material with a sharp switching threshold. Selective erasure is done by electrically switching the film to $+P_r$ and illuminating the bits to be reset, which puts them back on the (+) curve.

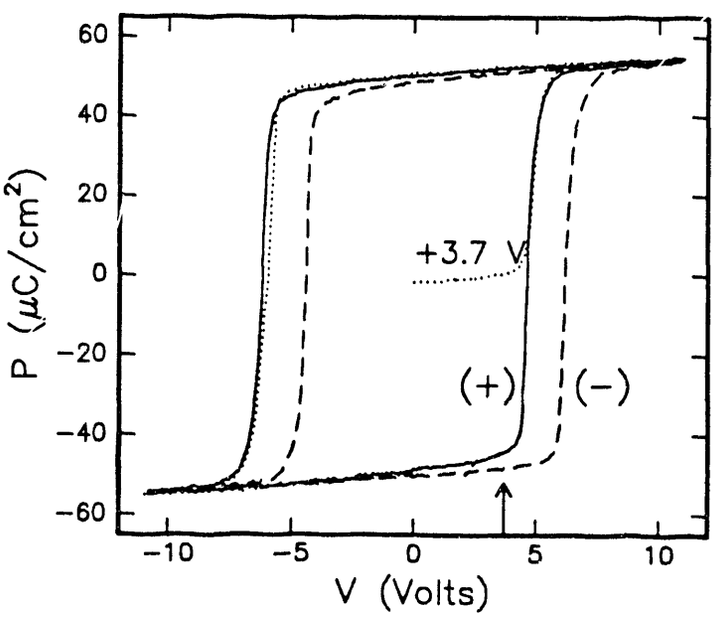

Figure 8. Photo-induced hysteresis response for operation of an optical memory. The arrow corresponds to 3.7 V, which switches the (+) state bits to $P_r \simeq 0$.

To read the polarization state of a bit, a focused laser with a longer wavelength than the writing light is used so that the read beam does not alter the polarization state. Using polarizing optics, the induced birefringence can be used to modulate the intensity of the

reflected read beam. Since the films exhibit an electrooptic response which is roughly quadratic with respect to polarization, the two desirable end-point states are $P_r = |P_r(max)|$ and $P_r = 0$. An alternative readout technique for determining the film polarization is the use of photocurrent or photovoltage measurements [9,25]. However, the photovoltage response is slow and the photocurrent response scales decreases linearly with decreasing sample area; consequently, these techniques are not be suitable for high-speed, high-density memories.

While a P(L)ZT thin-film optical memory could be implemented, many issues must be resolved to produce a competitive technology. First, the time constant for writing needs to be reduced by nearly two orders of magnitude. Therefore, it is critical to determine the rate-limiting process and to develop strategies for modifying the response time. A PZT optical-memory medium should also be compatible with solid-state lasers (λ = 700-800 nm), since these lasers are the basis of current magnetooptic memories. At this point, improvements in the photosensitivity at longer wavelengths are anticipated based on the improvements achieved in PLZT ceramics by ion implantation [26]. The minimum bit size also needs to be evaluated. The bit resolution may depend on both the grain size and the spreading of photo-induced carriers. Finally, the issues common to ferroelectric nonvolatile memories, such as retention, fatigue, and polarization-state imprinting, need to be considered for an optical memory.

CONCLUSIONS

Two different photo-induced changes in hysteresis behavior were characterized in PZT and PLZT films. The observed effects are controlled by the trapping of charge at the near surface region and/or at internal domain boundaries. Both of the observed photo-induced hysteresis changes are stable and reproducible and, thus, can be used to devise a working optical memory.

In addition, a waveguide refractometry technique was used to characterize the electric-field-induced changes in the principal refractive indices of PZT films. Application of an electric field sufficient to induce polarization saturation in a PZT 53/47 film leads to a negative uniaxial birefringence of $\Delta(n_e-n_o) = -0.021$. Furthermore, the ratio of the extraordinary to ordinary refractive index change ($\Delta n_e/\Delta n_o$) was found to be roughly -4/1, which implies that mechanisms other than simple domain reorientation contribute to the electrooptic response. Understanding these mechanisms will be important for improving the electrooptic response for optical readout.

In conclusion, many issues need to be resolved to develop a technology that can compete with magnetooptic or magnetic memories. First, the photosensitivity needs to be improved with respect to both the time and spectral dependence. Improvements in the intrinsic photosensitivity of films can be anticipated from chemical doping or ion implantation. Confirming these anticipated improvements will be critical to the development of ferroelectric film optical memories. Second, the minimum bit size needs to be evaluated as compared to the diffraction limit. Third, issues common to ferroelectric memories, such as, retention, fatigue, and polarization-state imprinting, need to be evaluated for an optically-addressed, optically-read memory.

ACKNOWLEDGEMENTS

This work was supported by the Office of Naval Research and the U.S. Department of Energy under contract DE-AC04-76DP00789. The authors would like to acknowledge C.H. Seager, R.W. Schwartz, and J.A. Bullington for helpful discussions and thank D. Goodnow and J. Kubas for technical assistance.

REFERENCES

1. B.A. Tuttle, MRS Bull., 12, [5], 40 (1987).
2. A.R. Tanguay, Opt. Eng., 24, [1], 2 (1985).
3. C.E. Land, Ceram. Trans., 11, 343 (1990).
4. A. Ersen, S. Krishnakumar, V. Ozguz, J. Wang, C. Fan, S. Esener, and S.H. Lee, Appl. Opt., 31, 3950 (1992).
5. S.J. Martin, M.A. Butler, C.E. Land, Elec. Lett., 24, 1486 (1988).
6. C.E. Land and P.S. Peercy, Ferroelectrics, 22, 677 (1978).
7. J.W. Burgess, R.J. Hurditch, C.J. Kirkby, and G.E. Scrivener, Appl. Opt., 15, 1550 (1976).
8. P.J. Chen and C.E. Land, J. Appl. Phys., 51, 4961 (1980).
9. D. Dimos and R.W Schwartz, Mat. Res. Soc. Symp. Proc., 243, 73 (1992).
10. C.E. Land, J. Am. Ceram. Soc., 72, 2059 (1989).
11. K.D. Preston and G.H. Haertling, Appl. Phys. Lett., 60, 2831 (1992).
12. W.-G. Luo, A.L. Ding, and R.T. Zhang, Proc. of the 8th IEEE ISAF '92, 19.
13. H. Adachi, T. Kawaguchi, K. Setsune, K. Ohji, and K. Wasa, Appl. Phys. Lett., 42, 867 (1983).
14. C.E. Land, P.D. Thacher, and G.H. Haertling, in Applied Solid State Science, ed. R. Wolfe, (Academic Press, NY, 1974), p. 137.
15. R.W. Schwartz, B.C. Bunker, D. Dimos, R.A. Assink, B.A. Tuttle, D.R. Tallant, and I.A. Weinstock, Int. Ferroelectrics, 2, 243 (1992).
16. R.A. Assink and R.W. Schwartz, Chem. of Mater., 5, 511 (1993).
17. B.G. Potter, Jr., M.B. Sinclair, and D. Dimos, Appl. Phys. Lett. (submitted).
18. B.A. Tuttle, J.A. Voigt, T.J. Garino, D.C. Goodnow, R.W. Schwartz, D.L. Lamppa, T.J. Headley, and M.O. Eatough, Proc. of the 8th IEEE ISAF '92, 344.
19. B.A. Tuttle, J.A. Voigt, and T.J. Headley, J. Am. Ceram. Soc., 76, 1537 (1993).
20. D. Dimos, W.L. Warren, C.H. Seager, B.A. Tuttle, and R.W. Schwartz, J. Appl. Phys. (submitted).
21. D. Dimos, W.L. Warren, B.A. Tuttle, Mat. Res. Soc. Symp. Proc., 310, (1993).
22. V.V. Prisedsky, V.I. Shishkovsky, V.V. Klimov, Ferroelectrics, 17, 465 (1978).
23. J. Robertson, W.L. Warren, D. Dimos, B.A. Tuttle, and D.M. Smyth, (in preparation).
24. D. Dimos, C.E. Land, and R.W. Schwartz, Ceram. Trans., 25, 323 (1992).
25. S. Thakoor, Appl. Phys. Lett., 60, 3319 (1992).
26. C.E. Land and P.S. Peercy, Ferroelectrics, 45, 25 (1982).

DATE
FILMED
12/14/93